

**LA-UR-20-28381**

Accepted Manuscript

# Characterization of Heparin's Conformational Ensemble by Molecular Dynamics Simulations and Nuclear Magnetic Resonance Spectroscopy

Garcia, Angel Enrique

Janke, Joel

Yu, Yanlei

Pomin, Victor

Zhao, Jing

Wang, Chunyu

Linhardt, Robert

Provided by the author(s) and the Los Alamos National Laboratory (2022-02-03).

**To be published in:** Journal of Chemical Theory and Computation

**DOI to publisher's version:** 10.1021/acs.jctc.1c00760

**Permalink to record:**

<http://permalink.lanl.gov/object/view?what=info:lanl-repo/lareport/LA-UR-20-28381>



Los Alamos National Laboratory, an affirmative action/equal opportunity employer, is operated by Triad National Security, LLC for the National Nuclear Security Administration of U.S. Department of Energy under contract 89233218CNA000001. By approving this article, the publisher recognizes that the U.S. Government retains nonexclusive, royalty-free license to publish or reproduce the published form of this contribution, or to allow others to do so, for U.S. Government purposes. Los Alamos National Laboratory requests that the publisher identify this article as work performed under the auspices of the U.S. Department of Energy. Los Alamos National Laboratory strongly supports academic freedom and a researcher's right to publish; as an institution, however, the Laboratory does not endorse the viewpoint of a publication or guarantee its technical correctness.

# Characterization of Heparin's Conformational Ensemble by Molecular Dynamics Simulations and Nuclear Magnetic Resonance Spectroscopy

J. Joel Janke,<sup>†</sup> Yanlei Yu,<sup>†</sup> Vitor H. Pomin,<sup>§</sup> Jing Zhao,<sup>†</sup> Chunyu Wang,<sup>†</sup> Robert J. Linhardt,<sup>†\*</sup> and Angel E. García<sup>‡\*</sup>

<sup>†</sup>Center for Biotechnology and Interdisciplinary Studies, Rensselaer Polytechnic Institute, Troy, NY, 12180

<sup>‡</sup>Center for Nonlinear Studies, Los Alamos National Laboratory, Los Alamos, NM, 87545

<sup>§</sup>Department of BioMolecular Sciences, University of Mississippi, Oxford, MS 38677

KEYWORDS: Molecular dynamics simulations, Nuclear magnetic resonance spectroscopy, Heparin, Arixtra, GLYCAM06, CHARMM36

The DOI assigned to this article is <https://doi.org/10.1021/acs.jctc.1c00760> .

LA-UR-20-28381

Prepared for *Journal of Chemical Theory and Computation*; Accepted 1/25/2022.

\*Corresponding authors Angel E. García <agarcia@lanl.gov> and Robert J. Linhardt <linhar@rpi.edu>

ABSTRACT: Heparin is a highly charged, polysulfated polysaccharide and serves as an anticoagulant. Heparin binds to multiple proteins throughout the body, suggesting a large range of potential therapeutic applications. Although its function has been characterized in multiple physiological contexts, heparin's solution conformational dynamics and structure-function relationships are not fully understood. Molecular dynamics (MD) simulations facilitate the analysis of a molecule's underlying conformational ensemble, which then provides important information necessary for understanding structure-function relationships. However, for MD simulations to afford meaningful results, they must both provide adequate sampling and accurately represent the energy properties of a molecule. The aim of this study is to compare heparin's conformational ensemble using two well-developed force fields for carbohydrates, known as GLYCAM06 and CHARMM36, using replica exchange molecular dynamics (REMD) simulations, and to validate these results with NMR experiments. The anticoagulant sequence, an ultra-low-molecular-weight heparin, known as Arixtra (fondaparinux, sodium), was simulated with both parameter sets. The results suggest that GLYCAM06 matches experimental nuclear magnetic resonance three-bond  $J$ -coupling values measured for Arixtra better than CHARMM36. In addition, NOESY and ROESY experiments suggest that Arixtra is very flexible in the sub-millisecond time scale and does not adopt a unique structure at 25 C. Moreover, GLYCAM06 affords a much more dynamic conformational ensemble for Arixtra than CHARMM36.

## Introduction

Glycosaminoglycans (GAGs) are polysaccharides with a repeating disaccharide unit of a hexuronic acid (or galactose in the case of keratan sulfate) and a hexosamine. There are six different types of GAGs: heparin, heparan sulfate, chondroitin sulfate, dermatan sulfate, hyaluronan, and keratan sulfate. GAGs are distinguished by several characteristics, including monosaccharide composition, number of disaccharide repeating units, overall negative charge, and the number and type of ring substituents. GAGs have been implicated in many physiological processes, including cell-cell communications, blood coagulation, and pathogenic infection, that are mediated through GAG interactions with proteins.<sup>1,2</sup>

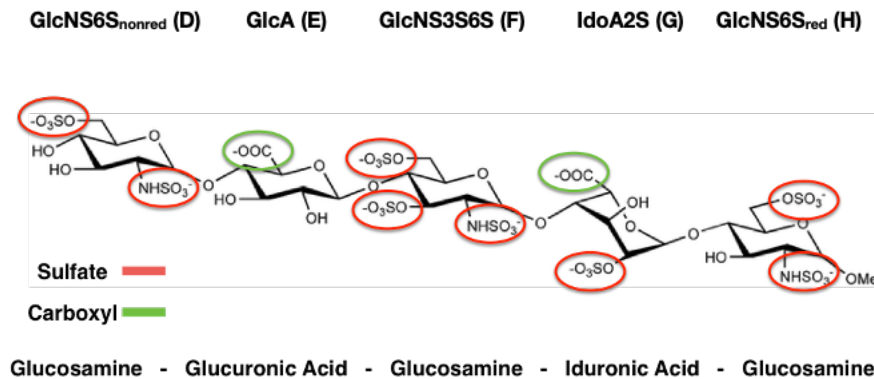


**Figure 1.** Chemical structure of Arixtra. The charged functional groups are circled in either green (carboxylate groups) or red (sulfates and sulfamates). Here, we used the disaccharide sequence (GlcNS6D-GlcA-GlcNS3S6S-IdoA2S- GlcNS6S) as well as the ring labels (D-E-F-G-H).

Heparin is a highly sulfated GAG and one of the most negatively charged molecules in the human body, with an average net charge of -3.5 due to the 2.5 sulfo groups and 1 carboxyl group on each disaccharide unit. The carboxyl group is present in the uronic acid residue and the sulfo groups decorate the hydroxyl and amino groups around heparin's pyranose rings. In addition to

these sulfo group substituents, either glucuronic acid or its C-5 epimer, iduronic acid, can result in a large number of different heparin sequences. As an anticoagulant, heparin interacts with antithrombin III (AT) in the coagulation cascade to prevent blood clotting.<sup>3</sup> A specific sequence motif in heparin (comprising Arixtra [Figure 1]) binds tightly to, and activates AT causing it to undergo a conformational change, while other heparin sequences may also bind but with much less affinity.<sup>4-9</sup> The unbound and bound conformations of AT can be compared to experimentally infer AT's conformational mechanism. However, a dynamic, high-resolution conformational mechanism relating heparin's sequence and the activation of AT has not been determined.

Nuclear magnetic resonance (NMR) spectroscopy has proven to be a useful tool for characterizing heparin's conformation and dynamics. Most notably, Mulloy and co-workers used a combined molecular modeling and NMR approach to show that canonical, trisulfated heparin forms a rodlike structure.<sup>10</sup> The details of their method involved measuring  $^3J$ -coupling constants to calculate dihedral angles and  $^1\text{H}$ - $^1\text{H}$  nuclear Overhauser effect (NOE) resonances to calculate inter-proton distances. With these distances, a molecular modeling approach was used to generate canonical heparin's conformation. This structure became the basis of many heparin computational studies.<sup>11-18</sup>

While heparin is a natural product consisting of a polydisperse, microheterogeneous mixture of polysaccharide chains, Arixtra is a synthetic, homogeneous pentasaccharide. This allows for more detailed structural studies and more informative molecular dynamics (MD) simulations. Beyond the  $^3J$ -couplings, little experimental research has been undertaken to determine the conformation of heparin on an atomistic level. However, NMR studies have been conducted on the heparin pentasaccharide sequence present in Arixtra, focusing on NMR chemical shifts and  $^3J$ -coupling constants.<sup>19-21</sup> One recent study by Beecher et al. showed experimental

evidence for a hydroxyl-oxygen-hydrogen bond within Arixtra.<sup>22</sup> Using a modified NMR nuclear Overhauser effect spectroscopy (NOESY) experiment (two-dimensional chemical exchange spectroscopy [EXSY]), this group characterized through-space interactions of the hydroxyl and sulfamate hydrogens of Arixtra with the surrounding water. Reduced interaction with the water suggests that one of the hydroxyl or sulfamate hydrogens was involved in a hydrogen bond, which suggests a potentially structurally important intramolecular hydrogen bond. Thus, using EXSY buildup curves and temperature coefficients, Beecher and co-workers inferred that the third ring hydroxyl on the uronic acids of Arixtra were most likely to be involved in an intramolecular hydrogen bond and found general agreement with MD simulations.<sup>22</sup> While hydrogen bonds may form within Arixtra, the degree to which hydrogen bonds contribute to a specific conformation (or conformational equilibrium) relative to other types of intramolecular interactions has not been determined.

Over the past several decades, MD simulations have provided a valuable tool for studying the conformational ensembles of all four biological macromolecules, lipids, proteins, carbohydrates, and nucleic acids. Several force fields have been parameterized for each type of macromolecule and these are continuously being improved. There are many examples of the types of problems solved using this approach, but, in the context of the current study, the most notable applications are those involving carbohydrate conformational ensembles.

Using replica exchange molecular dynamics (REMD) simulations,<sup>23</sup> we simulated Arixtra with the GLYCAM06 and CHARMM36 force fields.<sup>23–25</sup> The fluctuations of the four glycosidic linkages and ring dynamics of Arixtra were examined using both force fields and then compared with previously published <sup>3</sup>*J*-coupling data (Fig. S2).<sup>21</sup> Comparison to experimental data showed that GLYCAM06 more closely approximates <sup>3</sup>*J*-coupling values for Arixtra than CHARMM36,

with most differences occurring in the conformational dynamics of the iduronic acid ring of Arixtra. Thus, while both force fields have been used for calculating carbohydrate properties, we find that, by comparison to currently available experimental data, GLYCAM06 provides a better description of the conformational properties of Arixtra.

## Methods

**Preparation of Arixtra.** Arixtra (fondaparinux, sodium) was purchased from AuroMedics Pharma LLC (East Windsor, NJ). The sample was desalted by dialysis using a 100-500 Da molecular-weight cutoff (MWCO) dialysis tube (Spectrum Laboratories, CA) against Millipore distilled water ( $\text{pH} = 6.89 \pm 0.04$ ) with a water exchange every day for 5 days. The dialyzed Arixtra was lyophilized before NMR spectra were collected.

**NMR Analysis of Arixtra.** Approximately 4 mg of Arixtra was dissolved in 550  $\mu\text{L}$  of “100%” (D 99.96%) deuterium oxide ( $\text{D}_2\text{O}$ ) and transferred to a 5 mm NMR tube (purchased from Cambridge Isotope Laboratories, Inc., Andover, MA). Then, a series of one-dimensional  $^1\text{H}$  and two-dimensional  $^1\text{H}$ - $^1\text{H}$  NMR spectra, including phase-sensitive NOESY (NOESYph), gradient-enhanced NOESYph (NOESYgpph), and rotating frame Overhauser effect spectroscopy (ROESY), were collected, at 25  $^\circ\text{C}$ , with multiple scans (16, 32, 64 and 128) and a Varian Inova 600 MHz magnet equipped with a triple resonance probe with field gradient coils. The two-dimensional NOESY and ROESY NMR spectra were recorded using a states-time proportion phase incrementation for quadrature detection in the indirect dimension. NOESY and ROESY spectra were run with  $1024 \times 256$  points. While ROESY spectra were recorded with 50, 100, 150, 200 and 300 ms spinlock, NOESY spectra were recorded with the following mixing times: 3, 5, 10, 15, 20, 25, and 50 ms.

Arixtra was prepared for NMR analysis by dialyzing the formulated drug product against water and lyophilized. After D<sub>2</sub>O exchange, a series of <sup>1</sup>H-based one-dimensional and two-dimensional (NOESY and ROESY) NMR spectra were collected at different numbers of scans and mixing times. The assignments of the resultant NMR signals were made using labels in the spectra using the notation A-G-A\*-I-A<sub>M</sub> of monosaccharides (from the nonreducing end to the reducing end) for the pentasaccharide structure of Arixtra. The signals of the one-dimensional NMR spectrum of Arixtra (Figure 2A) were fully and unequivocally identified based on their expected multiplicity patterns and typical <sup>1</sup>H chemical shift values as seen in previous works.<sup>20,26</sup> All <sup>1</sup>H chemical shift values of Arixtra collected at 25 °C are presented in Table S1. Besides confirmation of the structural integrity of the pentasaccharide sequence and assignments of the NMR <sup>1</sup>H line positions of Arixtra, the one-dimensional <sup>1</sup>H NMR spectrum was also quite valuable for assessing the purity of the sample. As shown in Figure 2A, almost all signals belong to the pentasaccharide structure of Arixtra, except those indicated by symbol “#”, which belong to glycerol, as one of the excipients found in commercial Arixtra. The low intensity of glycerol as compared to that of Arixtra demonstrates a high purity level of the current NMR preparation.

**System Setup and Simulation Parameters.** Arixtra was simulated using two different force field parameter sets, GLYCAM06 (with the parameters for sulfates published in 2016) and CHARMM36.<sup>24,25,27</sup> These parameter sets were chosen since both have previously parameterized heparin monosaccharides with which one can build Arixtra. Simulation engines were chosen so that they would natively implement the force fields. As a result, AMBER14 was used for simulations with GLYCAM06j-1 and NAMD 2.10 with CHARMM36.<sup>24,28,29</sup> For simulations of Arixtra with GLYCAM06, the topology was prepared using *tleap*.<sup>30</sup> Water molecules (1,972

TIP3P) were placed around Arixtra in the shape of a periodic truncated octahedron with a water buffer defined so that Arixtra was at least 8.5 Å from the nearest box edge. The CHARMM36 simulations were set up using CHARMM40b2 and placed within a periodic rhombic dodecahedron box and simulated with NAMD 2.10<sup>25,28,31,32</sup> with 1,788 CHARMM TIP3P water molecules.<sup>33</sup> For both systems, 10 sodium ions were added to neutralize the system. No excess salt was added to the simulated systems since it mimics the minimal salt conditions of the desalted Arixtra used in the experiments.

Simulation parameters were selected to follow the parameters chosen for each respective force field given in their original publications. For the GLYCAM06 simulation, the system was run with a time step of 2 fs, which is allowed due to the SHAKE constraints implemented for carbon-hydrogen bonds.<sup>34</sup> The nonbonded cutoff was set to 10 Å for both PME electrostatic and Lennard-Jones interactions.<sup>35,36</sup> The GLYCAM06 simulations began with 10000 steps of minimization (5000 steps of steepest descent followed by 5000 steps of conjugate gradient minimization). After this, the system was heated for 1 nanosecond to 300 K using the NVT ensemble (Berendsen thermostat) followed by a 1 nanosecond run where the pressure was equilibrated to 1 atm using the NPT ensemble.<sup>37</sup> Following this, the temperature- and pressure-equilibrated Arixtra system was used as the starting point for 32 temperature replicas that were run for 750 ns each, yielding a total sampling of 24 μs. The Langevin dynamics were used for the REMD simulations with a collision frequency of 1 ps<sup>-1</sup>.<sup>38</sup>

The CHARMM36 simulations were run with NAMD 2.12.<sup>25,28</sup> As was the case for the GLYCAM06 simulations, the CHARMM36 systems were energy-minimized, temperature-equilibrated for 1 nanosecond to 300 Kelvin using the NVT ensemble, and pressure-equilibrated for 1 nanosecond to 1 atm using the NPT ensemble, followed by 750 ns of NVT T-REMD

simulations using 30 temperature-replicas. The minimization involved 1000 steps of conjugate gradient minimization. The Langevin thermostat was used for the temperature and pressure equilibrations as well as the NVT T-REMD simulations with a collision frequency of 1 ps<sup>-1</sup>. SHAKE constraints were used, which allowed a time step of 2 fs. For the NPT pressure equilibration, Langevin piston Nose-Hoover method was used to keep the pressure constant at 1 atm, with a Langevin piston period of 100 fs, a Langevin piston decay of 50.0 fs, and a Langevin piston temperature of 300 K.<sup>39</sup> For both PME electrostatics and Lennard-Jones interactions, a cutoff of 12 Å was used and was subjected to a switching function from 10 to 12 Å.

**Temperature-Replica Exchange Molecular Dynamics.** Temperature-replica exchange molecular dynamics (T-REMD) is an enhanced sampling simulation method that allows faster convergence of a system's degrees of freedom than that of standard molecular dynamics simulations.<sup>23</sup> For T-REMD, a series of replica systems are run in parallel where each replica runs at a particular temperature and neighboring replicas may exchange temperatures.

Prior to performing T-REMD simulations, Arixtra was equilibrated at 300 K under NVT conditions for 1 nanosecond and then equilibrated under NPT conditions at 300 K and 1 atm. These equilibrated configurations were then used as a starting point for T-REMD simulations under NVT conditions. For both force fields, a temperature range of 275 - 454.97 K was used to generate 32 and 30 replicas for GLYCAM06 and CHARMM36, respectively. We used the method of Hecce et al. to generate temperatures for T-REMD that maintain a acceptance exchange probability of approximately 25%.<sup>40</sup> The temperatures used to simulate Arixtra in both GLYCAM06 and CHARMM36 are in Table S2. For each replica in both the GLYCAM06 and CHARMM36 T-REMD systems, the replicas were sampled for 750 ns per replica, and the final 500 ns per replica was used for analysis. Figure S2 shows that the 750 ns REMD simulations allow for multiple

cycles through the temperature range and that all replicas (walker) contribute proportionally to the 300K ensemble used for calculating averages.

**Dihedral Principal Component Analysis.** Dihedral principal component analysis (dPCA) was used where the conformations of the carbohydrate were described by linear eigenvector projections based on glycosidic dihedral fluctuations to characterize the populations of various Arixtra conformations.<sup>41</sup> dPCA was used to represent carbohydrate conformations instead of Cartesian PCA since dPCA separates internal motion from the overall motion which provides a clearer view conformational motion of Arixtra around glycosidic dihedrals. We used the program cpptraj from AmberTools to calculate the dPCA.

dPCA is accomplished by first converting dihedral angles into polar coordinates and diagonalizing the covariance matrix of the polar coordinates. The eigenvectors of the matrix correspond to components which are ranked according to the amplitude of the eigenvalue. Accordingly, the component (or principal component) with the largest eigenvalue corresponds to the largest fluctuations. As a result, the first two principal components are used to describe the conformational changes around the glycosidic torsions. The free energy landscapes of the conformational motion of Arixtra, were then computed by using the natural logarithm of the densities of the first two principal components.

$$\Delta A = -RT \ln(P),$$

where  $R$  is the gas constant,  $T$  is the temperature, and  $P$  is the fraction that a given state is occupied. DBSCAN clustering of the dPCA results was then used to describe the Arixtra conformations within each dPCA free energy minimum.<sup>42</sup>

**Experimental Validation.** We compared the calculated three-bond  $J$ -coupling values to the measured values in the literature to assess whether the REMD results agreed with experimental data. Three-bond  $J$ -couplings are measured through NMR spectroscopy, and they represent the coupled nature of atomic spins three bonds apart. Since a three-bond  $J$ -coupling is based on nuclear

spins three bonds apart, the value of a three-bond  $J$ -coupling is also correlated with their corresponding dihedral angles.<sup>43</sup> While dihedral angles cannot be directly measured from an NMR experiment, three-bond  $J$ -couplings can be measured as splitting between NMR peaks within appropriate NMR spectra and dihedral angles can be solved from the  $J$ -coupling values using the Karplus equation.<sup>44</sup>

Thus, in the following manner, the Karplus equation allows calculation of a three-bond  $J$ -coupling from a dihedral angle in the following form:

$$J = A \cos^2 \theta + B \cos \theta + C$$

where  $A$ ,  $B$ , and  $C$  are constants that can be parameterized from either empirical data or theoretical calculations where both  $J$  and  $\theta$  are known.<sup>44-46</sup>

Karplus equations with two different set of coefficient  $A$ ,  $B$  and  $C$  were used in this study, one for the glycosidic bonds and another for intraring dihedral angles. These two equations were necessary because the measured three-bond  $J$ -couplings for the glycosidic bonds are heteronuclear  $J$ -couplings and the measured  $J$ -couplings for intraring dihedrals are homonuclear  $J$ -couplings and these represent two different types of three-bond  $J$ -couplings. The glycosidic bond three-bond  $J$ -couplings were measured between the carbon and hydrogen atoms (thus, the term “heteronuclear” three-bond  $J$ -coupling) and the intraring dihedrals are measured between two hydrogen atoms (termed a three-bond “homonuclear”  $J$ -coupling). A search of previously published literature yielded Karplus equations for both the intraring and the glycosidic bond dihedral angles.<sup>47,48</sup> The Karplus equation for the homonuclear intraring  $J$ -couplings was parameterized by Hricovini and Bizik who used density functional theory to calculate GAG three-bond  $J$ -couplings for a range of homonuclear dihedral angles.<sup>48</sup> Their resulting Karplus equation was then the following:

$$J = 9.6 \cos^2 \theta - 0.6 \cos \theta + 0.2$$

Tvaroska and co-workers used experimental data to parameterize the Karplus equation for heteronuclear three-bond  $J$ -couplings across glycosidic bonds, yielding the following equation:<sup>47</sup>

$$J = 5.7 \cos^2 \theta - 0.6 \cos \theta + 0.5$$

These two Karplus equations were then used in this study for the comparison of experimental and theoretical three-bond  $J$ -couplings for both the glycosidic bonds and the intraring dihedrals. Average  $J$ -coupling values were calculated over the last 500 ns of the simulations, using the 300K ensembles. Error bars were calculated by performing 10 ns block averages over the last 500 ns of the simulations, and calculating the standard deviation of the block averages. The time block average was determined from the  $J$ -coupling correlation time using the method of Flyvbjerg and Petersen.<sup>49</sup>

## Results and Discussion

The role of Arixtra as an anticoagulant drug is well established, making Arixtra a valuable system for studying carbohydrate structure-function relationships. While a static structure of the conformation of Arixtra in complex with its target protein, antithrombin-III (AT), has been determined through X-ray crystallography, additional information is required to construct a more complete structure-function relationship for Arixtra in the context of its interaction with AT. One approach would be to study the conformational changes that occur in AT after binding to Arixtra.<sup>50,51</sup> Another possible way of understanding the structure-function relationship of Arixtra is to study the solution conformation of Arixtra prior to binding to AT and how much these conformations contribute to the role of Arixtra in anticoagulation.

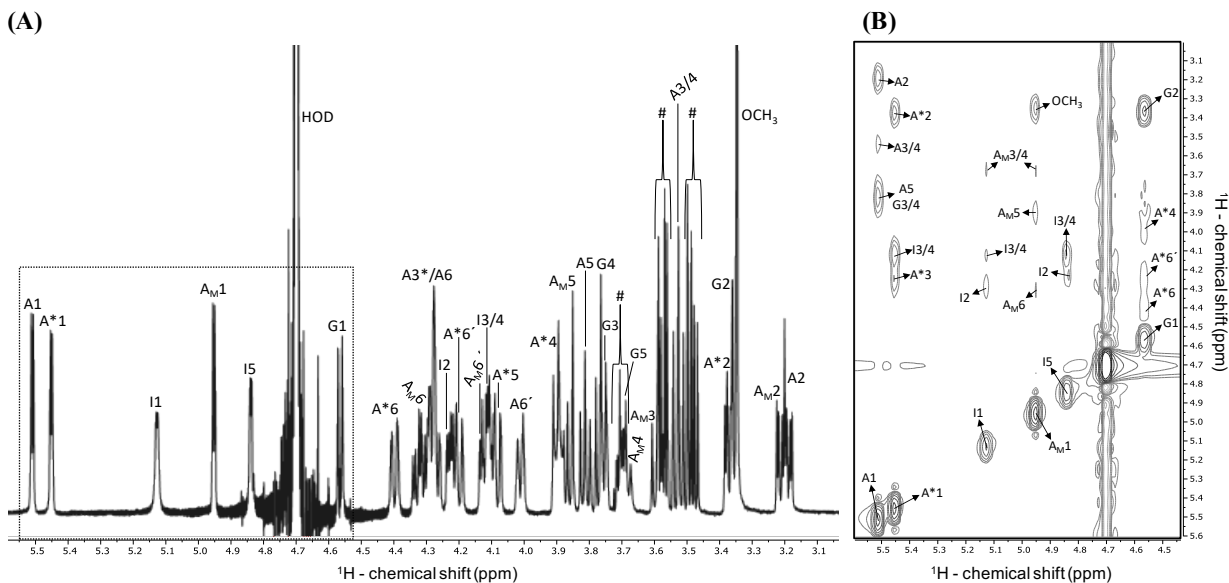


**Figure 2.** (A) One-dimensional  $^1\text{H}$  ( $\delta_{\text{H}}$  expansion from  $\sim 5.6$  to  $\sim 3.0$  ppm) and (B) two-dimensional  $^1\text{H}$ - $^1\text{H}$  ROESY ( $\delta_{\text{H}}$  expansions from  $\sim 5.6$  to  $4.5$  ppm, f2, and from  $\sim 5.6$  to  $\sim 3.0$  ppm, f1) NMR spectra of Arixtra dissolved in 100%  $\text{D}_2\text{O}$  (pH 4.29), and recorded at  $25^\circ\text{C}$  in a Varian 600 MHz NMR spectrometer.

A few and weak through-space  $^1\text{H}$ - $^1\text{H}$  cross-peaks were observed in all NOESY spectra collected at the various mixing times and multiple scan numbers. This indicates that the NOE signals of Arixtra fall inside or close to the region of low or null signal intensities in the curve of NOE's as a function of rotational correlation time. As a consequence, ROESY pulse sequence was selected as the preferable two-dimensional NMR method for the assessment of through-space  $^1\text{H}$ - $^1\text{H}$  contacts of Arixtra in solution. Among all spinlock times used (50, 100, 150, 200, and 300 ms), 200 ms has provided the best spectral profile. Figure 2B depicts the partial ROESY spectrum of Arixtra (downfield  $^1\text{H}$  anomeric region highlighted in the one-dimensional  $^1\text{H}$  NMR spectrum at Figure 2A) obtained at 200 ms and fully assigned regarding all its  $^1\text{H}$ - $^1\text{H}$  ROE pairs, even those of weak intensity (interproton distances in the range of  $3.7$ - $6.0$  Å). A few ambiguous assignments exist due to the high-order chemical shift degeneracy observed in NMR analysis of medium-sized sulfated oligosaccharides (10.1021/ac401791h). These peaks are A3/4 with  $\delta_{\text{H}}$  at 3.53 ppm, G3/4

with  $\delta_H$  at 3.75 and 3.77 ppm, I3/4 with  $\delta_H$  at 4.11 ppm and A<sub>M</sub>3/4 with  $\delta_H$  at 3.61/3.68 ppm (Table S1).

From the suite of ROE signals observed in the spectrum of Figure 2B, we can clearly see that almost all through-space interproton connections detectable by solution NMR of Arixtra analyzed at this spectral window, belong to either intra-residue contacts or inter-residue contacts primarily involved in the glycosidic linkages of the composing disaccharides (A1-G4 with  $\delta_H/\delta_H$  at 5.51/3.77 ppm, G1-A\*4 with  $\delta_H/\delta_H$  at 4.57/3.90 ppm, A\*1-I4 with  $\delta_H/\delta_H$  at 5.45/4.11 ppm, and I1-A<sub>M</sub>4  $\delta_H/\delta_H$  at 5.13/3.68 ppm). The only exception, although very weak, is the contacts seen between the anomeric <sup>1</sup>H of the GlcA unit (G1) and the two hydrogens at the C6 position of the adjacent trisulfated GlcN unit (A\*) with  $\delta_H/\delta_H$  at 4.57/4.40 and 4.57/4.20 ppm. This is expected considering the mobility of the CH<sub>2</sub>OSO<sub>3</sub><sup>-</sup> group outside the ring of the GlcNS3S6S (F) unit.

Based on this set of NMR-derived through-space signals, no clear folded 3D structure has been observed for Arixtra in solution at 25 °C. NOESY/ROESY-related conformational NMR studies of biomolecules in solution can suffer from some technical limitations. Besides sensitivity, some of these limitations are the NMR time scale (which ranges between seconds and milliseconds), the observation of only NMR resonances which ultimately resulted from an ensemble- and time-averaged of multiple conformers of Arixtra in solution, and the lifetime and abundance of such conformers in solution. These technical limitations of NMR spectroscopy usually make it very hard to detect conformations that might occur faster than the millisecond time scale and in relatively low abundance. Hence, alternative analytical methods, such as those based on computational calculations, must be employed.

Computational approaches provide an atomistic approach to characterize the conformation distribution of Arixtra. However, since carbohydrate force field parameters are relatively untested,

a comparison of the best force field parameters for modeling Arixtra becomes necessary using rigorous simulations. When this study was undertaken, two force fields provided parameters for Arixtra, one being the GLYCAM06 force field (compatible with the AMBER12SB protein force field) and the CHARMM36 force field.<sup>52</sup> Thus, the topic of this study is to rigorously compare these two force fields in the context of published experimental NMR data.

Using T-REMD simulations, our results showed that Arixtra exists as a conformational equilibrium between multiple conformations that includes flexibility in both the glycosidic bonds and within the 6-membered rings. Here, we analyze the structural ensembles sampled by Arixtra with two different force fields, using dihedral principal component analysis, end-to-end distance distributions, Ramachandran-like maps, and <sup>3</sup>J-coupling parameters. We then validate the <sup>3</sup>J-coupling parameters with experimental results.

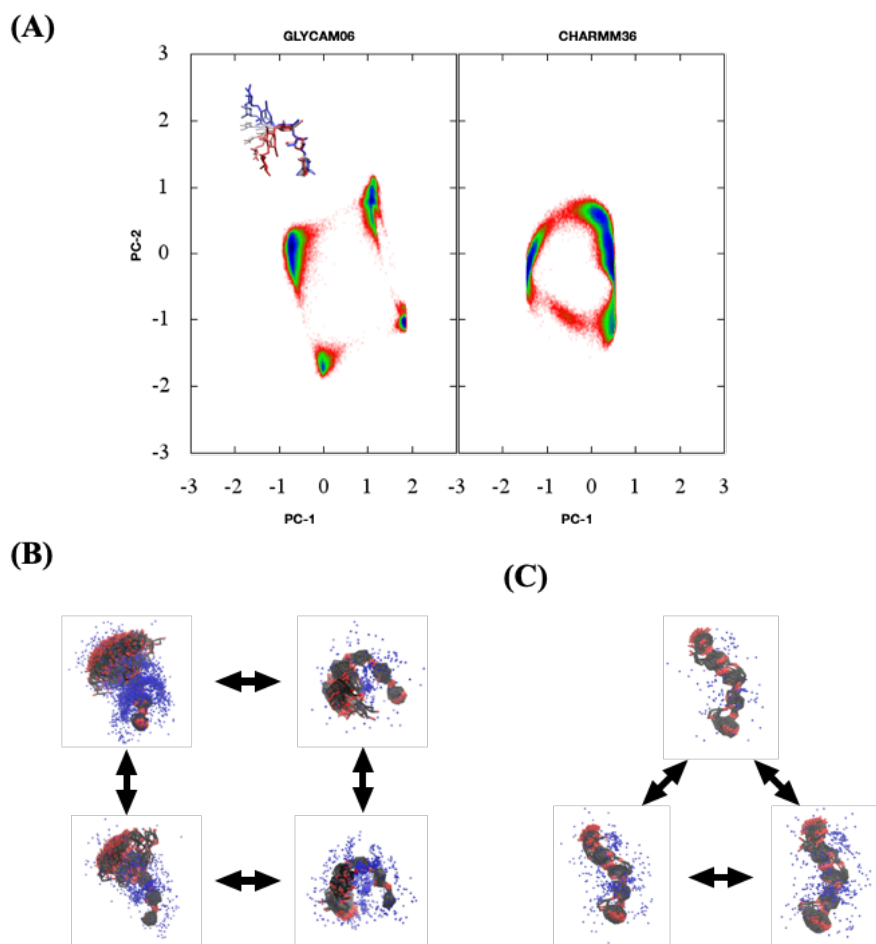
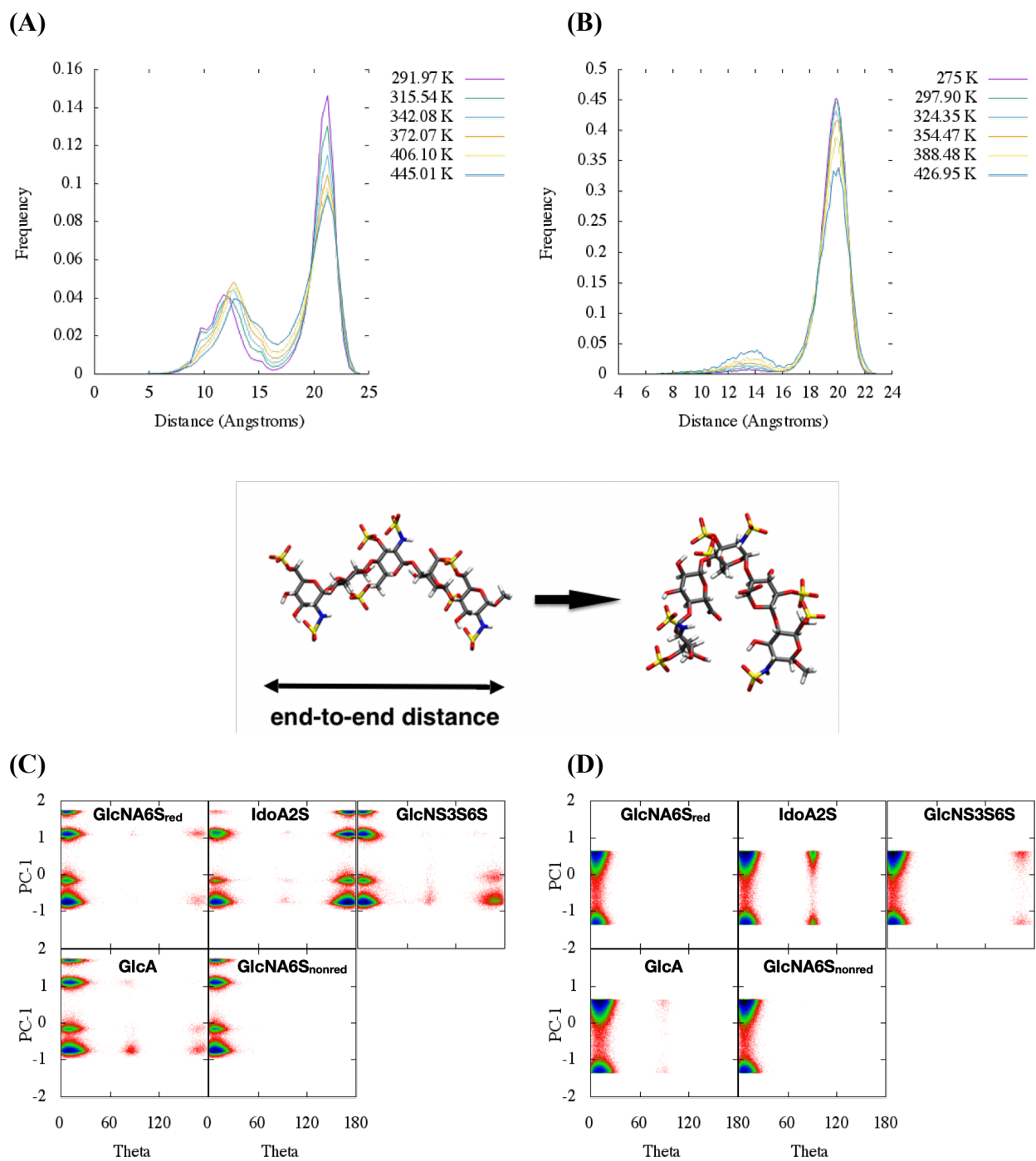


Figure 3: (A) The sampled energy landscape of Arixtra at approximately 300 K represented by dihedral principal component analysis (dPCA) based on the fluctuations of the glycosidic dihedrals. The left plot corresponds to the dPCA calculation for GLYCAM06, and the right plot corresponds to the dPCA calculation for CHARMM36. Clustering of the dPCA show conformations of Arixtra in the local free energy minima shown in above for (B) the GLYCAM06 force field and (C) the CHARMM36 force field. The blue dots represent the position of Na ions around Arixtra.

Dihedral principal component analysis was applied to the glycosidic bonds to obtain an easier visualization of glycosidic bond fluctuations. With the assumption that motion around the glycosidic bond explains much of the overall motion of Arixtra, DBSCAN clustering was applied to the first two principal components to extract the configurations of Arixtra that arise from dPCA.<sup>53</sup> Applying this approach to the T-REMD results from both GLYCAM06 and CHARMM36 allows comparison of the structural properties of Arixtra within each force field (Table S3). From this analysis, it is clear that the four GLYCAM06 dPCA populated states correspond to two

“kinked” molecular conformations and two “extended” conformations, which come about through twisting around dihedral 1 and dihedral 5 (see Figure 3B and 3C for images of the structures of Arixtra in each force field). In GLYCAM06, the first principal component (PC-1) corresponds to the extension and bending of Arixtra while the second principal component (PC-2) corresponds to twisting around the reducing of Arixtra. For CHARMM36, the dPCA free energy landscape shows three extended conformations where both the first two principal components describe twisting around the nonreducing end of Arixtra. Thus, using dPCA based on the glycosidic bonds of Arixtra yields useful configurational properties for comparison of the GLYCAM06 and CHARMM36 force fields.



**Figure 4.** (A) End-to-end distance distributions as a function of temperature for Arixtra obtained by MD simulations with two different force fields. The left (A) shows the melting curve for GLYCAM06 during T-REMD. Each line represents a temperature between 270 K and 456 K, showing that the free energy landscape becomes “flatter” with increasing temperature, allowing more conformational flexibility. The right (B) shows T-REMD simulations for CHARMM36 along the same temperature range, which shows that CHARMM36 did not melt in the same way as GLYCAM06 and remained relatively extended from high to low temperature. The relationship between the conformational changes in Arixtra and the ring puckering of each of the 6-membered

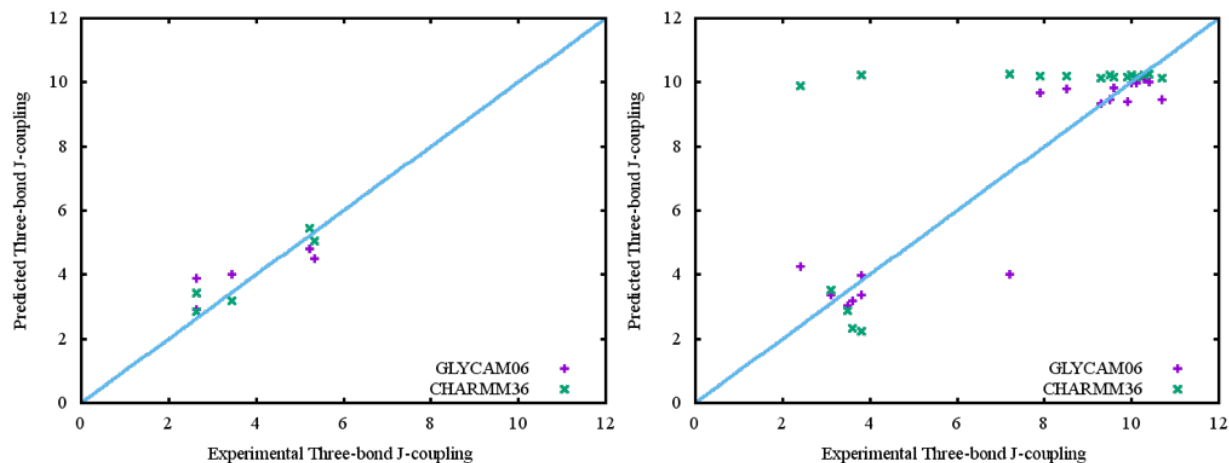
rings within Arixtra at approximately 300 K for (C) the GLYCAM06 force field and (D) the CHARM36 force field. The y-axis is the dPCA first principal component as a function of the Cremer-Pople spherical ring-puckering coordinate, theta, on the x-axis.

The end-to-end distance of Arixtra is provided in Figure 3A. The end-to-end distance of Arixtra is defined as the distance from the first ring carbon (C1) of the reducing end to the fourth ring carbon (C4) of the nonreducing end. The probability distribution of the end-to-end distance for both force fields is also provided in Figure 4A. Our simulations show that the CHARMM36 and GLYCAM06 yield significantly different end-to-end distributions for Arixtra. In particular, the Arixtra model based on GLYCAM06 show a multimodal distribution for the end-to-end distance, ranging from approximately 6 Å to 24 Å. The CHARMM36 distribution for the end-to-end distance is chiefly unimodal with a polymer length of approximately 20 Å and another, much smaller peak at approximately 13 Å. The dPCA representation in Figure 3A highlights each of these conformations in each force field, showing the usefulness of dPCA for describing the conformation of Arixtra compared to using individual structural properties like end-to-end distance or Ramachandran-like dihedrals shown next.

The glycosidic dihedrals from CHARMM36 and GLYCAM06 were next visualized using Ramachandran-like plots. These plots are generated by plotting the eight pairs of phi and psi dihedrals of the four glycosidic bonds of Arixtra against each other (Fig. S1). Plotting all the phi/psi dihedrals on a single plot suggests that CHARMM36 phi/psi dihedrals explore a greater configurational space than GLYCAM06 dihedrals. However, plotting the phi/psi dihedrals of each glycosidic bond separately shows that most of the flexibility in CHARMM36 is due to the glycosidic dihedrals closest to the nonreducing end of Arixtra, and there is clear flexibility in link 3 for GLYCAM06 which, due to the glycosidic dihedral's central location in Arixtra, explains the extension and bending seen in the GLYCAM06's dPCA results. Link 3 in CHARMM36 also

suggests flexibility, but, as can be seen from the end-to-end distance plot for CHARMM36, a bent conformation that may exist, but its population is negligible.

Cremer-Pople coordinates provide a spherical coordinate system that may describe the ring conformations within Arixtra.<sup>54</sup> While the conformation of a six-membered ring may be represented by six dihedral angles, Cremer-Pople ring puckering coordinates reduce the number of dimensions necessary to represent a ring to three “spherical” ring puckering coordinates, which represent all possible ring conformations. Thus, plotting the spherical Cremer-Pople coordinates theta versus phi provides sufficient information to differentiate between chair, boat, and skew boat conformations that appear when a ring flips from one chair conformation into an inverse chair conformation. Plotting theta against the first principal component from the dPCA analysis in Figures 4B and 4C shows that the ring conformations are related to the overall conformation of Arixtra, particularly that of GlcA and GlcNS3S6S which have more <sup>1</sup>C<sub>4</sub> ring conformations when the overall conformation of Arixtra is extended.



	GLYCAM06	CHARMM36
RMSE to Exp't J-couplings	1.02	2.32

**Figure 5.** Comparison of theoretical and experimental three-bond  $J$ -coupling values obtained in MD simulations using CHARMM36 (green) and GLYCAM06 (purple) force fields. The three-bond  $J$ -couplings that correspond to glycosidic bonds are on the left, and the three-bond  $J$ -couplings that correspond to ring dihedrals are on the right.

Three-bond  $J$ -couplings provide a useful metric for comparing dihedral motion to experimental values, since three-bond  $J$ -couplings can be directly measured by NMR and are trigonometrically related to dihedrals. Through comparison to  $J$ -couplings, homonuclear three-bond  $J$ -couplings which correspond to ring dihedrals shows that GLYCAM06 more closely approximates the experimental NMR data than CHARMM36 (Figure 5), especially those homonuclear three-bond  $J$ -couplings that correspond to the ring of iduronic acid (Supp. Table S4).<sup>21</sup> On the other hand, the heteronuclear three-bond  $J$ -couplings that correspond to the glycosidic bonds closely match experimental values for both CHARMM36 and GLYCAM06 (Figure 5).

IdoA2S (2-*O*-sulfo-L-idouronate) is known for its conformational equilibrium between a chair and skew-boat conformation (i.e., ring puckering).<sup>55–57</sup> Ring puckering can occur whether iduronic acid is 2-sulfated or unsulfated. Using three-bond  $J$ -couplings, multiple papers have

measured the ring puckering equilibrium of iduronate (or iduronic acid) and published experimental data for ring puckering equilibrium in iduronic acid as a monomer and in the context of heparin and other heparin variants.<sup>19,21,56</sup> In recent years, it has been argued that GLYCAM06's description of the ring puckering of IdoA2S is imperfectly described when compared to NMR results.<sup>58,59</sup> However, the limited ring puckering observed with CHARMM36 compared to GLYCAM06, demonstrates that GLYCAM06, while perhaps imperfect, represents better the IdoA2S ring dynamics.

Another interesting difference between the force fields is that CHARMM36's glycosidic flexibility is on the nonreducing end of Arixtra, while GLYCAM06's flexibility is both at the center of Arixtra and at the reducing end. This leads to dramatically different conformational profiles, where CHARMM36 Arixtra appears extended with twisting around its nonreducing end and GLYCAM06 Arixtra is in equilibrium between dominant extended conformations and minor bent conformations.

Recent studies compared the performance of other heparin sequences in GLYCAM06 and CHARMM36. One of these studies concluded that GLYCAM06 and CHARMM36 are highly similar based on simulations of a canonical heparin hexasaccharide.<sup>60</sup> There could be multiple reasons for why Nagarajan and co-workers came to the opposite conclusion of the current study. First, Nagarajan and co-workers only simulated their system for 20 ns from the same initial configurations for both GLYCAM06 and CHARMM36. Thus, limited sampling may not have allowed the hexasaccharide to sufficiently sample its conformational landscape, giving the appearance that the force fields were highly similar. Also, end-to-end distance and the minimum volume enclosing ellipsoid were the reaction coordinates used by Nagarajan and co-workers to describe the conformational ensemble of heparin. In the current study, we show that the end-to-

end distance may fail to capture many relevant conformations of a heparin oligosaccharide, since some conformations may have nearly identical end-to-end distances. Minimum volume enclosing ellipsoid may, to some degree, remedy this problem but would still suffer from a similar degeneracy. Thus, Nagarajan and co-workers might have benefitted from analyzing their results in terms of dihedral principal component analysis which reports on local angle fluctuations, in addition to the analysis they reported.

The second study by Balogh and co-workers compared GLYCAM06 and CHARMM36, using Gaussian-accelerated molecular dynamics simulations of a variant of Arixtra known as idraparinux.<sup>61</sup> This study also contained NOESY data for intraring distances that they used to conclude that CHARMM36 was the superior force field for simulating heparin. When comparing the methods and results of this study to the current one, several questions become apparent. In addition to the different kind of MD simulation method used, this study used a different reaction coordinate to describe the conformation of heparin, choosing ring dynamics over the Ramachandran-like dihedrals. In contrast, the current study analyzed both ring dynamics and the Ramachandran-like dihedrals. Also, we showed significant differences in flexibility when comparing the same glycosidic linkages across the two force fields. As a result, comparison of this work with the results from Balogh et al.<sup>61</sup> suggests that additional work is needed to assess carbohydrate force fields for additional sequences of heparin with a consistent MD method and reaction coordinate.<sup>46</sup> Balogh et al. recently published MD simulations of idraparinux with CHARMM36, examining the correlation between the glycosidic dihedrals and ring conformations. They also examined the kinetics of idraparinux's glycosidic bond fluctuations using Markov state models, finding faster fluctuations on the reducing end than the nonreducing end of idraparinux.<sup>62</sup>

It should be noted that  $J$ -couplings are degenerate inasmuch as a single three bond  $J$ -coupling can represent one of multiple possible dihedral angles. For this reason, it is desirable to compare MD simulation values to additional experimental data, such as nuclear Overhauser effect spectroscopy or residual dipolar couplings. In the absence of this experimental data, we suggest the use of GLYCAM06 for future calculations, particularly since the difference in homonuclear three-bond  $J$ -couplings is pronounced.

When comparing the glycosidic bonds of the two force fields there is a clear difference in how the two force fields behave (Figure 5). However, both still provide three-bond  $J$ -couplings that approximate the experimental data fairly well. This is likely due to the degeneracy of the  $J$ -couplings.

NMR studies were undertaken to validate the force fields. We looked at NOESY and ROESY spectra with multiple mixing times and found that our results are consistent with our hypothesis that GLYCAM06 is a better model than CHARMM36, but we could not definitely identify the bent conformation in the NMR that appears in the GLYCAM06 simulations, since it is likely that the bent conformations exist on sub-millisecond time scales. However, two ROESY cross peaks are consistent with the bent conformations that appear in the GLYCAM06 simulations, but these cross peaks have alternative assignment possibilities that are more plausible since they are shorter range than those that would correspond to a bent conformation. Future studies involving a 3D  $^{13}\text{C}$  NOESY of  $^{13}\text{C}$ -labeled Arixtra may resolve this difficulty and validate the existence of bent conformations. In addition, residual dipolar coupling NMR measurements would be useful to counterbalance the degeneracy in the three-bond  $J$ -couplings.

Although NMR is the best experimental approach for atomic-level resolution studies of flexible biomolecules, it is difficult to measure minor conformations within flexible molecules due

to time- and ensemble-averaging within the NMR measurement. Thus, since NMR measurements are in the millisecond time scale regime, NMR may not provide the necessary information.

## Conclusions

The performance of GLYCAM06 and CHARMM36 have been compared in this study. Although neither force fields yield three-bond  $J$ -coupling values that fully match experimental results, GLYCAM06 more closely matches experimental results than CHARMM36, particularly for the ring dihedrals of IdoA2S. Less flexibility in the ring of CHARMM IdoA2S likely contributes to a much poor comparison to three-bond  $J$ -coupling values than the GLYCAM06 IdoA2S, which is much more flexible. Also, NMR NOESY cannot capture the dynamic information of the bent versus extended conformations of GLYCAM that fluctuate on the microsecond time scale. Therefore, future NMR studies involving a 3D  $^{13}\text{C}$  NOESY of  $^{13}\text{C}$ -labeled Arixtra as well as residual dipolar couplings may provide the experimental information necessary to measure the minor bent conformations of Arixtra.

Rigorously testing two popular carbohydrate force field parameters for heparin is useful for determining which force field to use in subsequent studies. Of particular interest is simulating heparin-protein binding and showing the effect of sequence on the conformational ensemble of heparin. As is usually the case for force field work, the carbohydrate force fields will continue to improve as has been seen for force fields for other macromolecules. GROMOS has recently released uronic acid parameters, which suggests that GROMOS may soon have sufficient force field parameters for simulating heparin.<sup>63</sup>

## **Supporting Information**

Measured Chemical Shifts data for Arixtra at 25 °C. Temperature schedules of the REMD simulations. Further characterization of the structure and energy landscape obtained with REMD simulations. The Supporting Information is available free of charge on the ACS Publications website (link to be determined).

Author's Information

## **Corresponding Authors**

Angel E. Garcia Tel: 1-505-665-3883 <agarcia@lanl.gov> and Robert J. Linhardt Tel: 1-518-276-3404 <linhar@rpi.edu>

## **Acknowledgements**

JJJ was partially supported by the NIH Training Grant T32 GM067545. AEG and JJJ were partially funded by U.S. DOE LDRD funds (Project XX01). We acknowledge the Extreme Science and Engineering Discovery Environment (XSEDE) for access to supercomputer resources. VHP was funded by NIH (1P20GM130460-01A1-7936, and 1R03NS110996-01A1), and the University of Mississippi.

## **Notes**

The authors declare no competing financial interest.

## Rereferences

- (1) Kamhi, E.; Joo, E. J.; Dordick, J. S.; Linhardt, R. J. Glycosaminoglycans in Infectious Disease. *Biol. Rev.* **2013**, *88* (4), 928–943. <https://doi.org/10.1111/brv.12034>.
- (2) Linhardt, R. J.; Toida, T. Role of Glycosaminoglycans in Cellular Communication. *Acc. Chem. Res.* **2004**, *37* (7), 431–438. <https://doi.org/10.1021/ar030138x>.
- (3) Björk, I.; Lindahl, U. Mechanism of the Anticoagulant Action of Heparin. *Mol. Cell. Biochem.* **1982**, *48* (3), 161–182. <https://doi.org/10.1007/BF00421226>.
- (4) Rosenberg, R. D.; Damus, P. S. The Purification and Mechanism of Action of Human Antithrombin Heparin Cofactor. *J. Biol. Chem.* **1972**, *248* (18), 6490–6505.
- (5) Villanueva, G. B.; Danishefsky, I. Evidence for a Heparin-Induced Conformational Change on Antithrombin III. *Biochem. Biophys. Res. Commun.* **1977**, *74* (2), 803–809. [https://doi.org/10.1016/0006-291X\(77\)90374-6](https://doi.org/10.1016/0006-291X(77)90374-6).
- (6) Thunberg, L.; Bäckström, G.; Lindahl, U. Further Characterization of the Antithrombin-Binding Sequence in Heparin. *Carbohydr. Res.* **1982**, *100* (1), 393–410. [https://doi.org/10.1016/S0008-6215\(00\)81050-2](https://doi.org/10.1016/S0008-6215(00)81050-2).
- (7) Atha, D. H.; Lormeau, J. C.; Petitou, M.; Rosenberg, R. D.; Choay, J. Contribution of 3-O- and 6-O-Sulfated Glucosamine Residues in the Heparin-Induced Conformational Change in Antithrombin III. *Biochemistry* **1987**, *26* (20), 6454–6461.
- (8) Olson, S. T.; Björk, I.; Sheffer, R.; Craig, P. A.; Shore, J. D.; Choay, J. Role of the Antithrombin-Binding Pentasaccharide in Heparin Acceleration of Antithrombin-

- Proteinase Reactions. Resolution of the Antithrombin Conformational Change Contribution to Heparin Rate Enhancement. *J. Biol. Chem.* **1992**, *267* (18), 12528–12538.
- (9) Jin, L.; Abrahams, J. P.; Skinner, R.; Petitou, M.; Pike, R. N.; Carrell, R. W. The Anticoagulant Activation of Antithrombin by Heparin. *Proc. Natl. Acad. Sci. U. S. A.* **1997**, *94* (26), 14683–14688. <https://doi.org/10.1073/pnas.94.26.14683>.
- (10) Mulloy, B.; Forster, M. J.; Jones, C.; Davies, D. B. Nmr and Molecular-Modelling Studies of the Solution Conformation of Heparin. *Biochem. J.* **1993**, *293* (3), 849–858.
- (11) Krieger, E.; Geretti, E.; Brandner, B.; Goger, B.; Wells, T. N.; Kungl, A. J. A Structural and Dynamic Model for the Interaction of Interleukin-8 and Glycosaminoglycans: Support from Isothermal Fluorescence Titrations. *Proteins Struct. Funct. Genet.* **2004**, *54* (4), 768–775. <https://doi.org/10.1002/prot.10590>.
- (12) Ricard-Blum, S.; Féraud, O.; Lortat-Jacob, H.; Rencurosi, A.; Fukai, N.; Dkhissi, F.; Vittet, D.; Imberty, A.; Olsen, B. R.; Van Der Rest, M. Characterization of Endostatin Binding to Heparin and Heparan Sulfate by Surface Plasmon Resonance and Molecular Modeling: Role of Divalent Cations. *J. Biol. Chem.* **2004**, *279* (4), 2927–2936. <https://doi.org/10.1074/jbc.M309868200>.
- (13) Verli, H.; Guimarães, J. A. Molecular Dynamics Simulation of a Decasaccharide Fragment of Heparin in Aqueous Solution. *Carbohydr. Res.* **2004**, *339* (2), 281–290. <https://doi.org/10.1016/j.carres.2003.09.026>.
- (14) Gandhi, N. S.; Mancera, R. L. Free Energy Calculations of Glycosaminoglycan - Protein Interactions. *Glycobiology* **2009**, *19* (10), 1103–1115.

<https://doi.org/10.1093/glycob/cwp101>.

- (15) Jin, L.; Hricovíni, M.; Deakin, J. A.; Lyon, M.; Uhrin, D. Residual Dipolar Coupling Investigation of a Heparin Tetrasaccharide Confirms the Limited Effect of Flexibility of the Iduronic Acid on the Molecular Shape of Heparin. *Glycobiology* **2009**, *19* (11), 1185–1196. <https://doi.org/10.1093/glycob/cwp105>.
- (16) Costa, M. G. S.; Batista, P. R.; Shida, C. S.; Robert, C. H.; Bisch, P. M.; Pascutti, P. G. How Does Heparin Prevent the PH Inactivation of Cathepsin B? Allosteric Mechanism Elucidated by Docking and Molecular Dynamics. *BMC Genomics* **2010**, *11* (5), 1–15. <https://doi.org/10.1186/1471-2164-11-S5-S5>.
- (17) Nieto, L.; Canales, Á.; Giménez-Gallego, G.; Nieto, P. M.; Jiménez-Barbero, J. Conformational Selection of the AGA\* IAM Heparin Pentasaccharide When Bound to the Fibroblast Growth Factor Receptor. *Chem. Eur. J.* **2011**, *17* (40), 11204–11209.
- (18) Ballut, L.; Sapay, N.; Chautard, É.; Imberty, A.; Ricard-Blum, S. Mapping of Heparin/Heparan Sulfate Binding Sites on Av $\beta$ 3 Integrin by Molecular Docking. *J. Mol. Recognit.* **2013**, *26* (2), 76–85. <https://doi.org/10.1002/jmr.2250>.
- (19) Torri, G.; Casu, B.; Gatti, G.; Petitou, M.; Choay, J.; Jacquinet, J. C.; Sinay, P. Mono- and Bidimensional 500 MHz <sup>1</sup>H-NMR Spectra of a Synthetic Pentasaccharide Corresponding to the Binding Sequence of Heparin to Antithrombin-III: Evidence for Conformational Peculiarity of the Sulfated Iduronate Residue. *Biochem. Biophys. Res. Commun.* **1985**, *128* (1), 134–140. [https://doi.org/10.1016/0006-291X\(85\)91655-9](https://doi.org/10.1016/0006-291X(85)91655-9).
- (20) Hricovíni, M.; Torri, G. Dynamics in Aqueous Solutions of the Pentasaccharide

- Corresponding to the Binding Site of Heparin for Antithrombin III Studied by NMR Relaxation Measurements. *Carbohydr. Res.* **1995**, *268* (2), 159–175.  
[https://doi.org/10.1016/0008-6215\(94\)00334-C](https://doi.org/10.1016/0008-6215(94)00334-C).
- (21) Hricovini, M. Solution Structure of Heparin Pentasaccharide: NMR and DFT Analysis. *J. Phys. Chem. B* **2015**, *119* (38), 12397–12409.
- (22) Langeslay, D. J.; Young, R. P.; Beni, S.; Beecher, C. N.; Mueller, L. J.; Larive, C. K. Sulfamate Proton Solvent Exchange in Heparin Oligosaccharides: Evidence for a Persistent Hydrogen Bond in the Antithrombin-Binding Pentasaccharide Arixtra. *Glycobiology* **2012**, *22* (9), 1173–1182. <https://doi.org/10.1093/glycob/cws085>.
- (23) Sugita, Y.; Okamoto, Y. Replica-Exchange Molecular Dynamics Method for Protein Folding. *Chem. Phys. Lett.* **1999**, *314* (1–2), 141–151.
- (24) Kirschner, K. N.; Yongye, A. B.; Tschampel, S. M.; González-Outeiriño, J.; Daniels, C. R.; Foley, B. L.; Woods, R. J. GLYCAM06: A Generalizable Biomolecular Force Field. Carbohydrates. *J. Comput. Chem.* **2008**, *29* (4), 622–655.  
<https://doi.org/10.1002/jcc.20820>.
- (25) Guvench, O.; Mallajosyula, S. S.; Raman, E. P.; Hatcher, E.; Vanommeslaeghe, K.; Foster, T. J.; Jamison, F. W.; MacKerell, A. D. CHARMM Additive All-Atom Force Field for Carbohydrate Derivatives and Its Utility in Polysaccharide and Carbohydrate-Protein Modeling. *J. Chem. Theory Comput.* **2011**, *7* (10), 3162–3180.  
<https://doi.org/10.1021/ct200328p>.
- (26) Pomin, V. H. NMR Chemical Shifts in Structural Biology of Glycosaminoglycans. *Anal.*

*Chem.* **2014**, *86* (1), 65–94.

- (27) Singh, A.; Tessier, M. B.; Pederson, K.; Wang, X. C.; Venot, A. P.; Boons, G. J.; Prestegard, J. H.; Woods, R. J. Extension and Validation of the GLYCAM Force Field Parameters for Modeling Glycosaminoglycans. *Can. J. Chem.* **2016**, *94* (11), 927–935. <https://doi.org/10.1139/cjc-2015-0606>.
- (28) Phillips, J. C.; Braun, R.; Wang, W.; Gumbart, J.; Tajkhorshid, E.; Villa, E.; Chipot, C.; Skeel, R. D.; Kalé, L.; Schulten, K. Scalable Molecular Dynamics with NAMD. *J. Comput. Chem.* **2005**, *26* (16), 1781–1802. <https://doi.org/10.1002/jcc.20289>.
- (29) Case, D. A.; Babin, V.; Berryman, J.; Betz, R. M.; Cai, Q.; Cerutti, D. S.; Cheatham III, T. E.; Darden, T. A.; Duke, R. E.; Gohlke, H. AMBER 14, 2014. *Univ. California, San Fr.* **2014**.
- (30) Case, D. A.; Darden, T.; Cheatham III, T. E.; Simmerling, C.; Wang, J.; Duke, R.; Luo, R.; Walker, R.; Zhang, W.; Merz, K. AmberTools15. Amber 2010.
- (31) Brooks, B. R.; Bruccoleri, R. E.; Olafson, B. D.; States, D. J.; Swaminathan, S.; Karplus, M. CHARMM: A Program for Macromolecular Energy, Minimization, and Dynamics Calculations. *J. Comput. Chem.* **1983**, *4* (2), 187–217. <https://doi.org/10.1002/jcc.540040211>.
- (32) Brooks, B. R.; Brooks, C. L.; Mackerell, A. D.; Nilsson, L.; Petrella, R. J.; Roux, B.; Won, Y.; Archontis, G.; Bartels, C.; Boresch, S.; Caflisch, A.; Caves, L.; Cui, Q.; Dinner, A. R.; Feig, M.; Fischer, S.; Gao, J.; Hodoscek, M.; Im, W.; Kuczera, K.; Lazaridis, T.; Ma, J.; Ovchinnikov, V.; Paci, E.; Pastor, R. W.; Post, C. B.; Pu, J. Z.; Schaefer, M.;

- Tidor, B.; Venable, R. M.; Woodcock, H. L.; Wu, X.; Yang, W.; York, D. M.; Karplus, M. CHARMM: The Biomolecular Simulation Program. *J. Comput. Chem.* **2009**, *30* (10), 1545–1614. <https://doi.org/10.1002/jcc.21287>.
- (33) Price, D. J.; Brooks III, C. L. A Modified TIP3P Water Potential for Simulation with Ewald Summation. *J. Chem. Phys.* **2004**, *121* (20), 10096–10103.
- (34) Ryckaert, J. P.; Ciccotti, G.; Berendsen, H. J. C. Numerical Integration of the Cartesian Equations of Motion of a System with Constraints: Molecular Dynamics of n-Alkanes. *J. Comput. Phys.* **1977**, *23* (3), 327–341. [https://doi.org/10.1016/0021-9991\(77\)90098-5](https://doi.org/10.1016/0021-9991(77)90098-5).
- (35) Lennard-Jones, J. E. On the Determination of Molecular Fields. II. From the Equation of State of Gas. *Proc. Roy. Soc. A* **1924**, *106*, 463–477.
- (36) Darden, T.; York, D.; Pedersen, L. Particle Mesh Ewald: An  $N \cdot \log(N)$  Method for Ewald Sums in Large Systems. *J. Chem. Phys.* **1993**, *98* (12), 10089–10092.
- (37) Berendsen, H. J. C.; Postma, J. P. M.; Van Gunsteren, W. F.; Dinola, A.; Haak, J. R. Molecular Dynamics with Coupling to an External Bath. *J. Chem. Phys.* **1984**, *81* (8), 3684–3690. <https://doi.org/10.1063/1.448118>.
- (38) Davidchack, R. L.; Handel, R.; Tretyakov, M. V. Langevin Thermostat for Rigid Body Dynamics. *J. Chem. Phys.* **2009**, *130* (23), 234101. <https://doi.org/10.1063/1.3149788>.
- (39) Evans, D. J.; Holian, B. L. The Nose-Hoover Thermostat. *J. Chem. Phys.* **1985**, *83* (4069–4074). <https://doi.org/10.1063/1.449071>.
- (40) Garcia, A. E.; Herce, H.; Paschek, D. Simulations of Temperature and Pressure Unfolding

- of Peptides and Proteins with Replica Exchange Molecular Dynamics. *Annu. Rep. Comput. Chem.* **2006**, *2*, 83–95.
- (41) Mu, Y.; Nguyen, P. H.; Stock, G. Energy Landscape of a Small Peptide Revealed by Dihedral Angle Principal Component Analysis. *Proteins Struct. Funct. Bioinforma.* **2005**, *58* (1), 45–52.
- (42) Ester, M.; Kriegel, H.-P.; Sander, J.; Xu, X. A Density-Based Algorithm for Discovering Clusters in Large Spatial Databases with Noise. In *Kdd*; 1996; Vol. 96, pp 226–231.
- (43) Feeney, J. The Use of Three-Bond Spin-Spin Coupling Constants in the Determination of Conformations of Molecules in Solution. *Proc. R. Soc. London. A. Math. Phys. Sci.* **1975**, *345* (1640), 61–72.
- (44) Karplus, M. Vicinal Proton Coupling in Nuclear Magnetic Resonance. *J. Am. Chem. Soc.* **1963**, *85* (18), 2870–2871. <https://doi.org/10.1021/ja00901a059>.
- (45) Bystrov, V. F. Spin—Spin Coupling and the Conformational States of Peptide Systems. *Prog. Nucl. Magn. Reson. Spectrosc.* **1976**, *10* (2), 41–82.
- (46) Karplus, M.; Anderson, D. H. Valence-Bond Interpretation of Electron-Coupled Nuclear Spin Interactions; Application to Methane. *J. Chem. Phys.* **1959**, *30* (1), 6–10.
- (47) Tvaroška, I.; Hricovíni, M.; Petráková, E. An Attempt to Derive a New Karplus-Type Equation of Vicinal Proton-Carbon Coupling Constants for COCH Segments of Bonded Atoms. *Carbohydr. Res.* **1989**, *189*, 359–362. [https://doi.org/10.1016/0008-6215\(89\)84112-6](https://doi.org/10.1016/0008-6215(89)84112-6).

- (48) Hricovini, M.; Bizik, F. Relationship between Structure and Three-Bond Proton-Proton Coupling Constants in Glycosaminoglycans. *Carbohydr. Res.* **2007**, *342* (6), 779–783. <https://doi.org/10.1016/j.carres.2007.01.003>.
- (49) Flyvbjerg, H.; Petersen, H. G. Error Estimates on Averages of Correlated Data. *J. Chem. Phys.* **1989**, *91* (1), 461–466.
- (50) Carrell, R. W.; Stein, P. E.; Fermi, G.; Wardell, M. R. Biological Implications of a 3 Å Structure of Dimeric Antithrombin. *Structure* **1994**, *2* (4), 257–270.
- (51) Horton, N. C.; Connolly, B. A.; Perona, J. J. Inhibition of Eco RV Endonuclease by Deoxyribo-3 '-S-Phosphorothiolates: A High-Resolution X-Ray Crystallographic Study. *J. Am. Chem. Soc.* **2000**, *122* (14), 3314–3324.
- (52) Maier, J. A.; Martinez, C.; Kasavajhala, K.; Wickstrom, L.; Hauser, K. E.; Simmerling, C. Ff14SB: Improving the Accuracy of Protein Side Chain and Backbone Parameters from Ff99SB. *J. Chem. Theory Comput.* **2015**, *11* (8), 3696–3713. <https://doi.org/10.1021/acs.jctc.5b00255>.
- (53) Hahsler, M.; Piekenbrock, M.; Doran, D. Dbscan: Fast Density-Based Clustering with R. *J. Stat. Softw.* **2019**, *91* (1), 1–30. <https://doi.org/10.18637/jss.v091.i01>.
- (54) Cremer, D.; Pople, J. A. A General Definition of Ring Puckering Coordinates. *J. Am. Chem. Soc.* **1975**, *97* (6), 1354–1358. <https://doi.org/10.1021/ja00839a011>.
- (55) Pol-Fachin, L.; Verli, H. Depiction of the Forces Participating in the 2-O-Sulfo- $\alpha$ -l-Iduronic Acid Conformational Preference in Heparin Sequences in Aqueous Solutions.

*Carbohydr. Res.* **2008**, *343* (9), 1435–1445.

- (56) Ferro, D. R.; Provasoli, A.; Ragazzi, M.; Torri, G.; Casu, B.; Gatti, G.; Jacquinet, J. C.; Sinay, P.; Petitou, M.; Choay, J. Evidence for Conformational Equilibrium of the Sulfated L-Iduronate Residue in Heparin and in Synthetic Heparin Mono- and Oligo-Saccharides: NMR and Force-Field Studies. *J. Am. Chem. Soc.* **1986**, *108* (21), 6773–6778.
- (57) Babin, V.; Sagui, C. Conformational Free Energies of Methyl- $\alpha$ -L-Iduronic and Methyl- $\beta$ -D-Glucuronic Acids in Water. *J. Chem. Phys.* **2010**, *132* (10), 03B602.
- (58) Sattelle, B. M.; Bose-Basu, B.; Tessier, M.; Woods, R. J.; Serianni, A. S.; Almond, A. Dependence of Pyranose Ring Puckering on Anomeric Configuration: Methyl Idopyranosides. *J. Phys. Chem. B* **2012**, *116* (22), 6380–6386.  
<https://doi.org/10.1021/jp303183y>.
- (59) Oborsky, P.; Tvaroska, I.; Kralova, B.; Spiwok, V. Toward an Accurate Conformational Modeling of Iduronic Acid. *J. Phys. Chem. B* **2013**, *117* (4), 1003–1009.  
<https://doi.org/10.1021/jp3100552>.
- (60) Nagarajan, B.; Sankaranarayanan, N. V.; Desai, U. R. Rigorous Analysis of Free Solution Glycosaminoglycan Dynamics Using Simple, New Tools. *Glycobiology* **2020**, *30* (8), 516–527.
- (61) Balogh, G.; Gyöngyösi, T.; Timári, I.; Herczeg, M.; Borbás, A.; Fehér, K.; Kövér, K. E. Comparison of Carbohydrate Force Fields Using Gaussian Accelerated Molecular Dynamics Simulations and Development of Force Field Parameters for Heparin-Analogue Pentasaccharides. *J. Chem. Inf. Model.* **2019**, *59* (11), 4855–4867.

<https://doi.org/10.1021/acs.jcim.9b00666>.

- (62) Balogh, G.; Gyöngyösi, T.; Timári, I.; Herczeg, M.; Borbás, A.; Sadiq, S. K.; Fehér, K.; Kövér, K. E. Conformational Analysis of Heparin-Analogue Pentasaccharides by Nuclear Magnetic Resonance Spectroscopy and Molecular Dynamics Simulations. *J. Chem. Inf. Model.* **2021**, *61* (6), 2926–2936.
- (63) Panczyk, K.; Gaweda, K.; Drach, M.; Plazinski, W. Extension of the GROMOS 56a6CARBO/CARBO\_R Force Field for Charged, Protonated, and Esterified Uronates. *J. Phys. Chem. B* **2018**, *122* (14), 3696–3710.

# Supplementary Materials for “Characterization of Heparin’s Conformational Ensemble by Molecular Dynamics Simulations and Nuclear Magnetic Resonance Spectroscopy”

J. Joel Janke,<sup>†</sup> Yanlei Yu,<sup>†</sup> Vitor H. Pomin,<sup>§</sup> Jing Zhao,<sup>†</sup> Chunyu Wang,<sup>†</sup> Robert J. Linhardt,<sup>†\*</sup>  
and Angel E. García<sup>†\*</sup>

The supplementary materials provide the measured Chemical Shifts data for Arixtra<sup>™</sup> at 25 °C, temperature schedules of the REMD simulations, and further characterization of the structure and energy landscape obtained with REMD simulations.

**Table S1.**  $^1\text{H}$  chemical shifts ( $\delta$ , ppm) of Arixtra<sup>TM</sup> at 25 °C.

Residue <sup>a</sup>	$\delta$ $^1\text{H}$ (ppm) <sup>b</sup>						
	H1	H2	H3	H4	H5	H6/H6'	OCH <sub>3</sub>
D	5.51	3.20	3.53	3.53	3.81	4.29/4.02	NA
E	4.57	3.36	3.75	3.77	3.69	NA <sup>c</sup>	NA
F	5.45	3.38	4.28	3.90	4.08	4.40/4.20	NA
G	5.13	4.24	4.11	4.11	4.84	NA	NA
H	4.95	3.22	3.61	3.68	3.85	4.33/4.13	3.35

<sup>a</sup>Pentasaccharide structure was assigned as D-E-F-G-H as shown for the Arixtra sequence in Figure 1, starting from its non-reducing end.

<sup>b</sup>Chemical shift values, obtained from Figure 1A, are relative to external trimethylsilylpropionic acid at 0 ppm. HOD signal resonates at 4.7 ppm at 25 °C and was used to calibrate spectra processed and analyzed at Mnova software.

<sup>c</sup>Not applicable.

**Table S2:** The temperatures used for the T-REMD calculations for both GLYCAM06 and CHARMM36 (in units of Kelvin) in order to maintain an exchange probability of 25% between neighboring replicas. Since the CHARMM36 system had more water molecules than the Glycam06 system. Therefore, we added two additional replicas to the GLYCAN system to span the same temperatures ( 275K to 410.97K) as the CHARMM36 system.

<b>GLYCAM06</b>	275	279.1	283.29	287.58	291.97	296.46
	301.07	305.78	310.6	315.54	320.6	325.78
	331.08	336.52	342.08	347.79	353.63	359.62
	365.77	372.07	378.53	385.15	391.96	398.94
	406.1	413.46	421.03	428.8	436.79	445.01

	453.47	454.97				
<b>CHARMM36</b>	275	279.3	283.74	288.32	293.04	297.9
	302.9	308.04	313.33	318.77	324.35	330.08
	335.95	341.97	348.15	354.47	360.95	367.59
	374.39	381.35	388.48	395.79	403.28	410.97
	418.85	426.95	435.26	443.81	452.61	454.97

**Table S3.** The structural features of Arixtra™ from GLYCAM06 and CHARMM36. Each cluster corresponds to the DBScan clustering of the dPCA results for each force field.

	GLYCAM06				CHARMM36		
Cluster No.	0	1	2	3	0	1	2
Frequency (%)	58.74	<b>24.41</b>	7.98	<b>8.87</b>	72.37%	20.90%	6.73%
Average Length	20.86 +/- 1.02	12.14 +/- 1.52	19.58 +/- 1.32	10.41 +/- 1.03	19.93 +/- 0.92	19.33 +/- 1.15	19.62 +/- 1.11
Coordination No.	4.06	6.36	3.76	8.42	3.20	2.98	3.20
Link 1 phi/psi	35.56,- 11.65	39.96,0.06	33.10,- <b>175.17</b>	23.52,- <b>178.26</b>	48.50,-2.12	49.16,-2.34	48.80,-1.47
Link 2 phi/psi	-39.11,- 16.54	-32.63,- 9.07	-35.13,- 18.86	-28.41,- 24.28	-53.01,- 12.69	-53.30,- 13.82	-53.66,- 14.62
Link 3 phi/psi	37.02,7.85	45.88,- <b>174.80</b>	41.10,11.19	48.55,- <b>173.70</b>	48.76,9.79	48.62,9.78	47.98,8.19
Link 4 phi/psi	-42.70,- 32.57	-40.85,- 33.11	-43.54,- 32.40	-41.96,- 31.99	<b>-41.68,-</b> <b>36.26</b>	<b>-33.06-</b> <b>152.66</b>	<b>-3.81,13.87</b>
RMSD to X-ray <sup>a</sup>	1.09 +/- 0.29	3.53 +/- 0.36	0.99 +/- 0.33	3.71 +/- 0.19	1.21 +/- 0.08	1.18 +/- 0.13	1.27 +/- 0.10

<sup>a</sup>The RMSD to X-ray is computed by taking the RMSD to carbon and oxygen atoms of the glycosidic bonds of

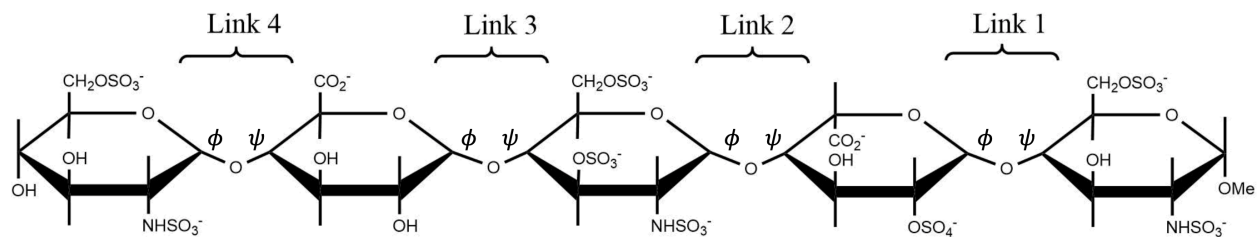
Arixtra™ bound to AT in PDB structure 3EVJ.

Table S4: The average three-bond  $J$ -couplings of Arixtra™ for GLYCAM06 and CHARMM36 calculated as described in the Methods section. The mean and standard deviation of the  $J$ -couplings were determined through block averaging.  $J$ -Couplings are reported in Hz.

<i>Residue</i>	<i>Torsion</i>	<i>GLYCAM</i>	<i>CHARMM</i>	<i>*Exp't <math>J^B</math></i>
<b>Homonuclear</b>				
<b>GlcNS6S<sub>red</sub> (H)</b>	H1-H2	3.18 ± 0.02	2.32 ± 0.01	3.6
	H2-H3	10.02 ± 0.17	10.25 ± 0.01	10.4
	H3-H4	9.80 ± 0.17	10.19 ± 0.00	8.5
	H4-H5	9.96 ± 0.18	10.20 ± 0.00	10.0
<b>IdoA2S (G)</b>	H1-H2	4.08 ± 0.72	10.23 ± 0.01	3.8
	H2-H3	4.11 ± 0.70	10.25 ± 0.00	7.2
	H3-H4	4.35 ± 0.71	10.02 ± 0.06	2.4
	H4-H5	3.38 ± 0.08	3.46 ± 0.02	3.1
<b>GlcNS3S6S (F)</b>	H1-H2	3.04 ± 0.09	2.85 ± 0.02	3.5
	H2-H3	9.44 ± 0.51	10.23 ± 0.00	10.7
	H3-H4	9.33 ± 0.51	10.22 ± 0.00	9.3
	H4-H5	9.38 ± 0.53	10.23 ± 0.00	9.9
<b>GlcA (E)</b>	H1-H2	9.67 ± 0.22	10.17 ± 0.01	7.9
	H2-H3	9.45 ± 0.17	10.17 ± 0.04	9.5
	H3-H4	9.58 ± 0.15	9.90 ± 0.09	N/A
	H4-H5	9.95 ± 0.17	9.97 ± 0.10	N/A
<b>GlcNS6S<sub>nonred</sub> (D)</b>	H1-H2	3.38 ± 0.03	2.18 ± 0.01	3.8
	H2-H3	10.09 ± 0.01	10.24 ± 0.00	10.3
	H3-H4	9.82 ± 0.01	10.16 ± 0.01	9.6
	H4-H5	9.97 ± 0.02	10.15 ± 0.01	10.1
<b>Heteronuclear</b>				
<b>G - H Linkage</b>	C1 (G) - H4 (H)	5.05 ± 0.14	5.27 ± 0.01	4.5
	H1 (G) - C4 (H)	3.44 ± 0.12	2.65 ± 0.01	2.9
<b>F - G Linkage</b>	C1 (F) - H4 (G)	4.43 ± 0.09	4.94 ± 0.03	N/A
	H1 (F) - C4 (G)	3.48 ± 0.12	2.33 ± 0.02	N/A
<b>D - F Linage</b>	C1 (E) - H4 (F)	5.43 ± 0.17	5.16 ± 0.02	4.8
	H1 (E) - C4 (F)	2.86 ± 0.08	2.52 ± 0.03	3.9
<b>D - E Linkage</b>	C1 (D) - H4 (E)	4.09 ± 0.08	4.19 ± 0.06	N/A
	H1 (D) - C4 (E)	3.17 ± 0.06	3.36 ± 0.03	4.0
<b>RMSE to Expt</b>		<b>0.92</b>	<b>2.13</b>	
<b>PCC to Expt</b>		<b>0.94</b>	<b>0.77</b>	

\* Available experimental three-bond  $J$ -couplings were published by Hricovini.<sup>21</sup> The experimental values reported by Hricovini<sup>21</sup> have a +/- 0.3 Hz error.

Figure S1: The structure of Arixtra™ with emphasis on the four glycosidic linkages numbered from the reducing end of the oligosaccharide.



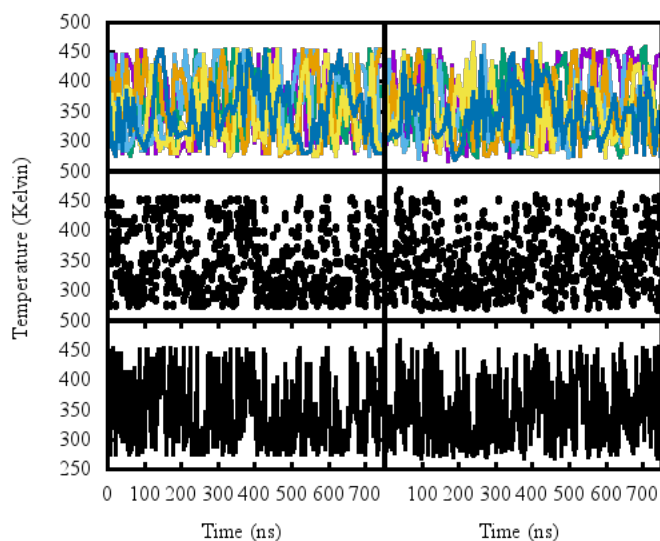
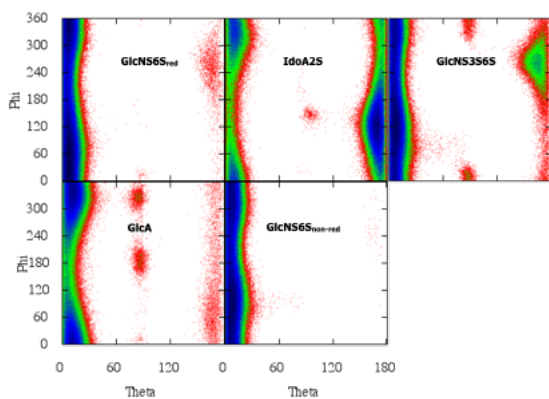


Figure S2: **Time series of the temperature for each replica during the calculations.** The curves for Glycam are on the left, for CHARMM on the right. The **top** plots show the temperature for selected replicas. The **middle** plots show temperature history for the walker that contributed most to the  $\sim 300$  K ensembles (#29 for Glycam; # 23 for CHARMM). The **bottom** plots show the replica number vs time that contributed to the ensemble near 300K (301 for Glycam, 297.9 for CHARMM). These plots show that the walkers temperature diffuse up and down through the temperature domain during the simulations and that all replicas contribute to the 300K ensemble.

(A)



(B)

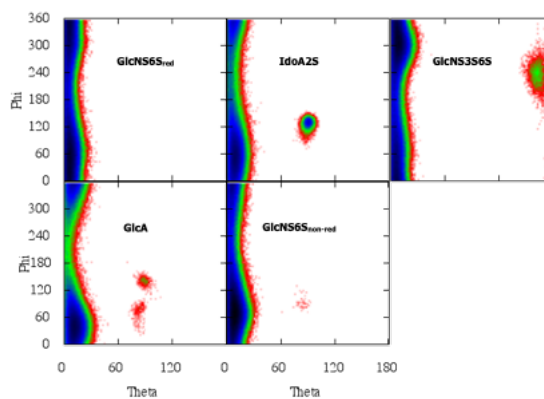
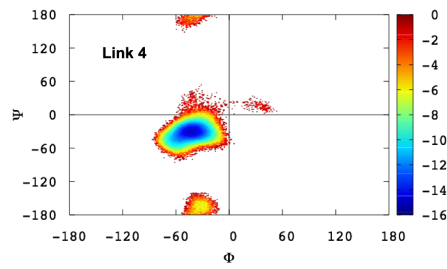
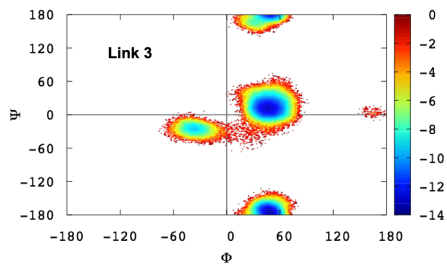
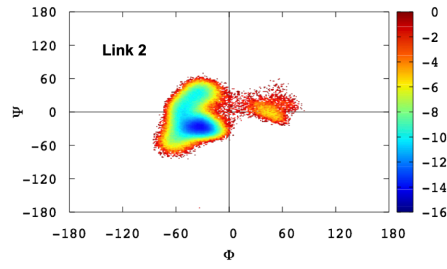
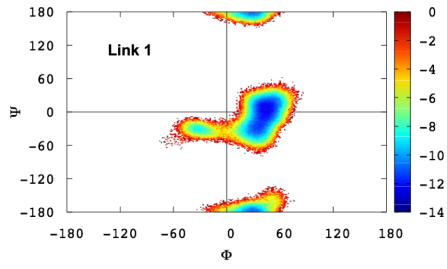


Figure S3: The ring pucker populations of each ring in Arixtra<sup>TM</sup> in the (A) GLYCAM06 and (B) CHARMM36 T-REMD simulations, expressed in Cremer-Pople ring pucker coordinates, theta and phi.

(A)



(B)

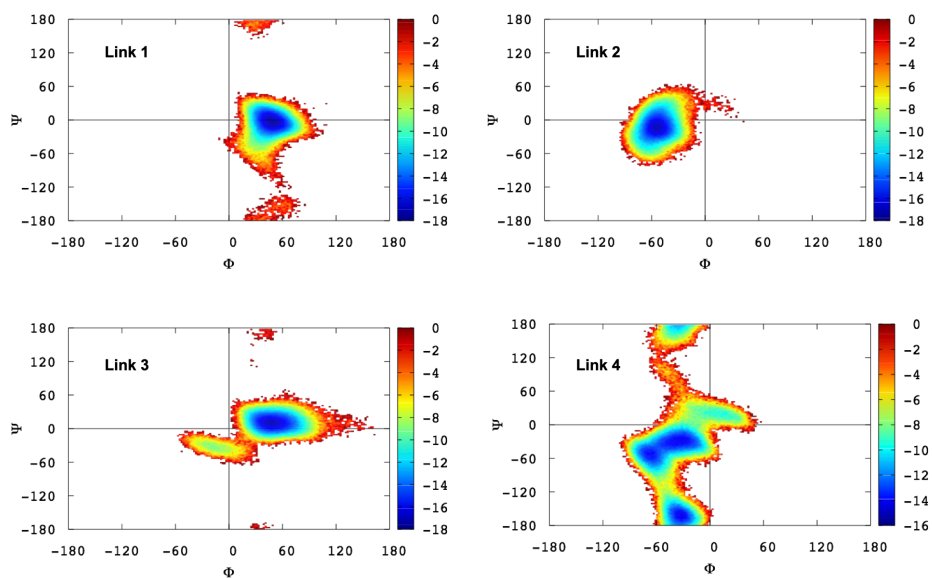


Figure S4: The Ramachandran-like plots of (A) GLYCAM06 and (B) CHARMM36 for Arixtra™ where each linkage corresponds to those highlighted in the structure of Arixtra™ in Figure S1. The legend corresponds to the free energy landscape in kJ/mol units.